Log law of the wall revisited in Taylor-Couette flows at intermediate Reynolds numbers

Harminder Singh and Claudio Alberto Torres Suazo
Postgraduate Program of Chemical Engineering, Universidade Federal de São Carlos, São Carlos-SP, Brasil

Alain Liné*
LISBP, Université de Toulouse, CNRS, INRA, INSA, Toulouse, France
(Received 28 July 2016; published 28 November 2016)

We provide Reynolds averaged azimuthal velocity profiles, measured in a Taylor-Couette system in turbulent flow, at medium Reynolds ($7800 < \mathrm{Re} < 18000$) number with particle image velocimetry technique. We find that in the wall regions, close to the inner and outer cylinders, the azimuthal velocity profile reveals a significant deviation from classical logarithmic law. In order to propose a new law of the wall, the profile of turbulent mixing length was estimated from data processing; it was shown to behave nonlinearly with the radial wall distance. Based on this turbulent mixing length expression, a law of the wall was proposed for the Reynolds averaged azimuthal velocity, derived from momentum balance and validated by comparison to different data. In addition, the profile of viscous dissipation rate was investigated and compared to the global power needed to maintain the inner cylinder in rotation.

DOI: 10.1103/PhysRevE.94.053120

I. INTRODUCTION

The present investigation is concerned with the experimental analysis of turbulent velocity field in a Taylor-Couette system. Such systems have many applications in chemical engineering [1,2], fluid mechanics [3,4], rotating machinery [5], biological applications [6,7], as well as astrophysics [8–10] and soft matter [11]. Since Taylor's first theoretical results (one century ago), a huge amount of work was dedicated to Taylor-Couette flow [12]. Taylor-Couette flow was qualified as one of the paradigmatic flows in physics of fluids [13,14]. It is considered to be among the most investigated problems in fluid mechanics. However, in spite of substantial work [15–17], basic questions related to the wall law of azimuthal velocity or near-wall turbulent structure dynamics remain unanswered. This paper will address azimuthal velocity profile at medium Reynolds number.

The geometrical parameters of a Taylor-Couette system are the inner, r_i, and outer, r_o, cylinder radii and its height, h. This leads to a gap width $d = r_o - r_i$, radius ratio $\eta = r_i/r_o$, and aspect ratio $\Gamma = h/b$. The radius ratio η accounts for the amount of curvature. For a given value of η, gravity being negligible, only the Reynolds (or Taylor) number is relevant to parametrize the hydrodynamics. The outer cylinder is at rest and the inner one is rotating. Its angular velocity is noted ωi and its rotational speed is N. One can thus define the Reynolds number, $\mathrm{Re} = r_i\omega(r_o - r_i)/\nu$, and Taylor number, $\mathrm{Ta} = \mathrm{Re}^2(1+\eta)^6/[4(2\eta)^4]$.

Different transport properties of Taylor-Couette system are based on the torque, which is needed to maintain the inner cylinder rotating at a constant angular velocity. The estimation of the torque can be performed using the dimensionless torque-G correlation, shown in Eq. (1), proposed by Wendt [18].

$$G = \begin{cases} 1.45\frac{\eta^{3/2}}{(1-\eta)^{7/4}}\mathrm{Re}^{1.5} & \text{for } 4\times10^2 < \mathrm{Re} < 10^4 \\ 0.23\frac{\eta^{3/2}}{(1-\eta)^{7/4}}\mathrm{Re}^{1.7} & \text{for } 10^4 < \mathrm{Re} < 10^5 \end{cases}. \quad (1)$$

Similar estimations of the torque can be obtained with more recent correlation proposed by Dubrulle and Hersant [19] and Paoletti *et al.* [20] who expressed the torque as a drag coefficient as shown in Eq. (2):

$$\frac{G}{\mathrm{Re}^2} = K_7\frac{\eta^2}{(1-\eta)^{3/2}}\frac{1}{\ln\left[\eta^2(1-\eta)\frac{\mathrm{Re}^2}{K_8}\right]^{3/2}}, \quad (2)$$

where the constants are given as $K7 = 0.4664$ and $K8 = 104$, (following Lewis and Swinney [21]). One can deduce from the knowledge of the torque, different characteristics such as inner wall shear stress, $\tau_{\omega i} = T/(2\pi r_i^2 h)$, (Pa), the outer wall shear stress, $\tau_{\omega o} = T/(2\pi r_o^2 h)$, (Pa), and the associated friction velocities at inner cylinder, $U_i^* = \sqrt{\tau_{\omega i}/\rho}$ and at outer cylinder, $U_o^* = \sqrt{\tau_{\omega o}/\rho}$, (m/s).

In this paper, local transport properties of Taylor-Couette flow are investigated through an experimental approach based on particle image velocimetry (PIV) measurements of instantaneous velocity field in a plane. The first issue of this paper is to investigate the azimuthal velocity profile; in particular, we are interested in the behavior of the azimuthal velocity in turbulent flow, in the boundary layer close to the wall. It is known for some time, since Smith and Townsend [22], that in a Taylor-Couette flow, "no significant region of logarithmic variation of velocity can exist" for "any flow Reynolds less than 20000." Indeed, a rather limited extent of the logarithmic region is exhibited at such Reynolds numbers [14,23,24]. However, the classical values of logarithmic law ($1/\kappa$ and B) do not provide a good fit with the data, both experimental data [13,16,21,22] and DNS simulations [4,25]. Huisman *et al.* [13] investigated highly turbulent Taylor-Couette flow (up to $\mathrm{Re} = 2\times10^6$). They observed log law in such ultimate Taylor-Couette regime. At lower Reynolds number, Ref. [14] performed experiments and reported that the azimuthal velocity profile does not follow a log law. They attributed this difference to nonlinear dependence of turbulent viscosity, and possibly to Taylor rolls. Ostilla Monico *et al.* [24] performed DNS simulations of Taylor-Couette flow. They concluded that the logarithmic layer is limited to a relatively small range of the domain, providing insufficient separation of length scales (less than half of a

*line@insa-toulouse.fr

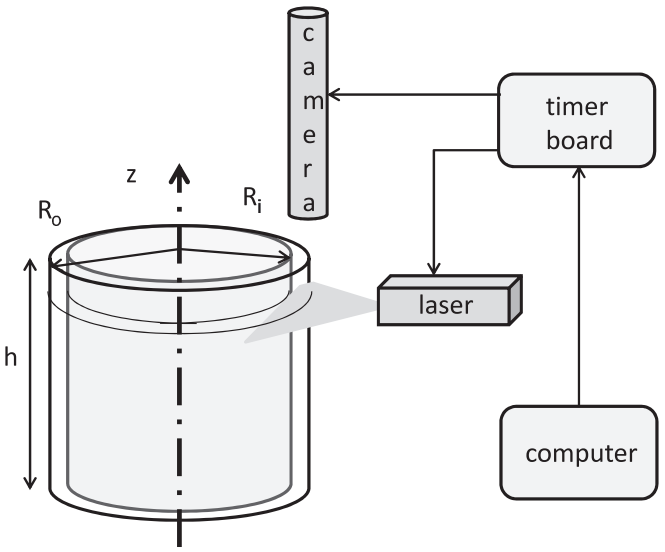

FIG. 1. Diagram of the setup.

decade) to exhibit near-wall cascade corresponding to fully developed log law profile.

In this paper, we will analyze the azimuthal velocity profile at medium Reynolds numbers and compare it to the log law; we will deduce from the measurements a profile of the mixing length. We will investigate whether (or not) linear (or nonlinear) dependence of mixing length with respect to wall distance is observed; based on these results, we will propose a new expression of the azimuthal velocity close to the cylinders and compare it to the Reynolds averaged azimuthal velocity.

The second issue is to relate the local hydrodynamics to the power needed to maintain the inner cylinder rotating at a constant angular velocity ω. The global power P (Watt) can be estimated from the knowledge of the torque, $P = T\omega$. An average value of the viscous dissipation rate of total kinetic energy $\langle\epsilon\rangle$ (W/kg) can then be deduced: $\langle\epsilon\rangle = P/[\rho\pi(r_o^2 - r_i^2)h]$. Assuming a logarithmic velocity profile for highly turbulent flow, Lathrop *et al.* [26] proposed a correlation to calculate the global torque. In this paper, we will derive the profile of viscous dissipation rate of the mean flow kinetic energy and we will estimate the viscous dissipation rate of the turbulent kinetic energy, assuming equilibrium between production and dissipation of turbulent kinetic energy. Finally, we will compare the average value of viscous dissipation rate of total kinetic energy to the global estimation $\langle\epsilon\rangle$ [Eq. (1)].

II. EXPERIMENTS

A. Description of the case setup

In our Taylor-Couette system (Fig. 1), the inner cylinder radius is $ri = 100$ mm and the outer one is $ro = 115$ mm; its height is $h = 200$ mm. This corresponds to a gap width, $d = 15$ mm, a radius ratio, $\eta = 0.87$, and an aspect ratio, $\Gamma = 13.3$.

The fluid is tap water. Four angular velocities of the inner cylinder, ωi, were investigated (see Table I). The respective values of the rotational speed N, Reynolds number Re, and Taylor number Ta are given in Table I, as well as hydrodynamic characteristics such as inner and outer wall shear stresses, inner U_i^* and outer U_o^* wall friction velocities. The torque T is estimated using Wendt correlation [Eq. (1)]. Global values such as the power P needed to maintain the inner cylinder rotating as well as the volume averaged viscous dissipation rate of the kinetic energy $\langle\epsilon\rangle$ are estimated. The volume averaged values of viscous dissipation rate of the kinetic energy $\langle\epsilon\rangle$ are compared to the local values at the inner cylinder.

Assuming linear azimuthal velocity radial profile $U_\theta(\delta)$ in the viscous sublayer (δ being the radial distance to the inner cylinder wall), $U_\theta(\delta)/U_i^* = \delta U_i^*/\nu$, the velocity gradient can be derived as $\partial U_\theta/\partial\delta = U_i^{*2}/\nu$ and the local values of viscous dissipation rate of the kinetic energy can be estimated at the inner cylinder as $\epsilon_i(\delta) = \nu(\partial U_\theta/\partial\delta)^2 = U_i^{*4}/\nu = \text{const}$. Its expression is thus given by $\epsilon_i = U_i^{*4}/\nu$, which constitutes a general expression of the viscous dissipation rate of kinetic energy at the wall in turbulent (viscous sublayer) or laminar flow (Poiseuille, Couette, steady-state pipe flow); these local values of ϵ_i are 23.5 to 14 times larger than the volume averaged values $\langle\epsilon\rangle$. In wall turbulence, in the logarithmic law region (region of equilibrium between production and dissipation of turbulent kinetic energy), the local dissipation rate is inversely proportional to the distance to the wall $\epsilon(\delta_i) = U_i^{*3}/(\kappa\delta_i) = U_i^{*4}/\nu/(\kappa\delta_i^+)$. Thus, at a distance such as $\delta_i^+ = 25$, the local dissipation rate of turbulent kinetic energy is equal to $\epsilon(\delta_i) = U_i^{*3}/(\kappa\delta_i) = U_i^{*4}/\nu/(\kappa\delta_i^+) = \epsilon_i/10$, thus 10 times smaller than the maximum value of dissipation rate at the wall. In Table I, averaged values of Kolmogorov microscales and Taylor microscales are also given; they will be used as an order of magnitude to estimate the range of length scales that may be filtered by the PIV technique.

It should be pointed out that the correlation proposed by Wendt gives an average torque whereas due to Taylor vortex structure, an axial dependence is expected. Consequently, the values of shear stresses at the inner and outer wall may be slightly biased. This will not be considered in the present paper. In the present work, radial profiles of Reynolds averaged azimuthal velocity are measured in a plane by PIV system and analyzed.

B. PIV system

The PIV system consists of a class IV Quantel Big Sky Laser (15 Hz and $\lambda = 532$ nm), FlowSense EO 16 MPixel camera (4872×3248) provided by Dantec Dynamics using a 60 mm objective having a diaphragm aperture of f/2.8 to f/32 and a synchronization system. The black colored internal cylinder is made of PVC, and the transparent external cylinder is made of Plexiglas. The Taylor-Couette (TC) system is placed in a parallelepiped box, filled with water to reduce optical problems. In the experiments reported here, limited to the analysis of the velocity field in horizontal planes, the camera was placed on the top of the Taylor-Couette system to capture the motion of particles in different horizontal planes. Between the camera and the chosen laser illuminated plane lies the fluid inside the TC system and above that plane, and the flat and transparent Plexiglas plate placed on the top of the TC.

The focusing of the camera in the respective plane is the first step of calibration, which was achieved by using a calibration plate made of quarter-circular flat plate of stainless

TABLE I. The global transport properties for the Taylor-Couette system.

Parameters (dimensions)	Value			
	114 (rpm)	90	70	50
Rotational speed, N (rpm)	114	90	70	50
Angular velocity, ω (rad/s)	11.94	9.43	7.33	5.24
Reynolds number, $\mathrm{Re} = r_i\omega(r_o - r_i)/\nu$	1.8×10^4	1.4×10^4	1.1×10^4	7.8×10^3
Taylor number, $\mathrm{Ta} = \mathrm{Re}^2(1+\eta)^6/[4(2\eta)^4]$	3.7×10^8	2.3×10^8	1.4×10^8	7.2×10^7
Torque, (Nm), T, using Eq. (1)	0.022	0.015	0.01	0.006
Tip speed, $r_i\omega$ (m/s)	1.19	0.94	0.73	0.52
Inner wall shear stress, $\tau_{wi} = \tau/(2\pi r_i^2 h)$ (Pa)	1.78	1.19	0.78	0.46
Outer wall shear stress, $\tau_{wo} = \tau/(2\pi r_o^2 h)$ (Pa)	1.35	0.9	0.59	0.35
Friction velocity at inner cylinder, $U_i^* = \sqrt{\tau_{wi}/\rho}$ (m/s)	0.042	0.035	0.028	0.021
Friction velocity at outer cylinder, $U_o^* = \sqrt{\tau_{wo}/\rho}$ (m/s)	0.037	0.03	0.024	0.019
Global power, $P = \tau\omega$ (Watt)	0.27	0.14	0.07	0.03
Global viscous dissipation rate of kinetic energy, $\langle\epsilon\rangle = P/[\rho\pi(r_o^2 - r_i^2)h]$ (W/kg)	0.132	0.07	0.035	0.015
Local viscous dissipation rate of kinetic energy, $\epsilon_i = U_i^* 4/\nu$ (W/kg)	3.1	1.4	0.6	0.2
Average Kolmogorov's microscale, $\langle\eta\rangle = (\nu^3/\langle\epsilon\rangle)^{\frac{1}{4}}$ (μm)	52.5	61.6	73.0	90.5
Average Taylor's microscale, $\langle\lambda\rangle = \sqrt{15\nu\overline{u_i^2}/\langle\epsilon\rangle}$ (mm)	1.3	1.4	1.5	1.7

steel, the inner radius being 1 mm larger than the inner cylinder and outer radius being 1 mm smaller than the outer cylinder. One face of this plate was marked with horizontal and vertical lines, 1 mm apart from each other, forming a 1 mm square grid. The camera was focused on this plate and the images were saved in the computer program as calibration images. Then the second step for calibrating the images was conducted by computing a scale factor on the saved calibrated images. This scale factor was estimated by selecting two points on the saved images of the plate, and the known distance between the two points was provided. This procedure allowed the computer program to estimate the scale factor between the pixels and mm values along with the clarity of the images in that particular plane. Different horizontal planes (and vertical ones not reported here) were investigated. The vertical distance between two parallel horizontal planes was set to 10 mm. The results presented here were selected for the axial location at which the profile for each rotational speed was the closest to the center of vortex region of a Taylor vortex observed by PIV acquisition in vertical plane. Accordingly, the center of vortex region was observed to be closest at the $Z_h = 0.675 \pm 0.005$ for the rotational speeds of 114, 90, and 70 rpms, and at $Z_h = 0.525 \pm 0.005$ for 50 rpm, respectively, (where $Z_h = z/h$). The spatial resolution based on these aspects for the rotational speeds of 114, 90, and 70 rpm was found to be 125 μm and 175 μm for the 50 rpm, respectively. It is smaller than the volume averaged Taylor micro-scale (close to 1 mm), indicating that estimations of rms values will be accurate (there is no filtering of energy contributing turbulent length scales). The spatial resolution is only two times larger than the volume averaged Kolmogorov scale. Local values of Kolmogorov scale may be five times smaller than the volume averaged one and thus the direct estimation of the viscous dissipation rate of turbulent kinetic energy may be tricky.

Silver coated glass beads of 10 μm size were used as seeding particles. A time-step size of 75, 75, 150, and 200 μs was used for the 114, 90, 70, and 50 rpm rotational speed, respectively, with the laser sheet thickness smaller than 1 mm. A total of 2500 image pairs were found to be more than sufficient for each angular velocity ω at each different horizontal locations to achieve the statistical convergence of the first- and second-order fluctuating velocity components. The acquired data was processed with an image acquisition system provided by Dantec Dynamics, Dynamicstudio V4.0. The vector analysis was conducted using the adaptive correlation with overlapping window of 0% and interrogation cell size of 16 pixels squared for high resolution.

C. Mean flow data

Mean flow data are expressed as Reynolds averaged values defined as follows [Eq. (3)]:

$$\overline{U_\theta}(r) = \frac{1}{N}\sum_{k=1}^{N} U_\theta^k(r). \tag{3}$$

Where U_θ^k stands for the kth measurement of the radial azimuthal velocity component. The number N of events fixed to 1000 is sufficiently large to reach a statistical converged mean. In Fig. 2, the Reynolds averaged azimuthal velocity $\overline{U_\theta}$ profile is plotted versus the radial distance to the wall δ, in basic geometrical units; the velocity scale is the inner cylinder velocity, usually named tip velocity, $U_{\mathrm{tip}} = \omega_i r_i$ and the length scale is the gap between the cylinders $d = r_o - r_i$. The azimuthal velocity profiles being selected in planes corresponding to the center of Taylor cells, the Reynolds averaged radial velocity is almost null. The azimuthal velocity profiles are plotted for the four angular velocities ω_i of the inner cylinder. The profiles are almost superimposed. The radial gradients of azimuthal velocity are high close to the inner and outer cylinders. Indeed, the Reynolds averaged azimuthal velocity profile presents distinct regions: near the inner and outer cylinders, a shear-driven boundary layer and in the bulk of the gap, the bulk velocity profile is flat and the azimuthal velocity $\overline{U_\theta}$ is close to $\omega_i/2$, half the angular velocities of the inner cylinder, agreeing with previous measurements of

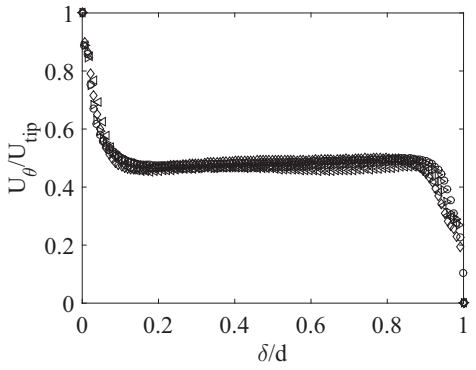

FIG. 2. Reynolds averaged azimuthal velocity $\overline{U_\theta}$ profile versus the radial distance to the wall δ for different impeller rotational speeds N: ○ 114 rpm, ▷ 90 rpm, ◇ 70 rpm, ◁ 50 rpm; the velocity scale is the inner cylinder velocity and the length scale is the gap between the cylinders.

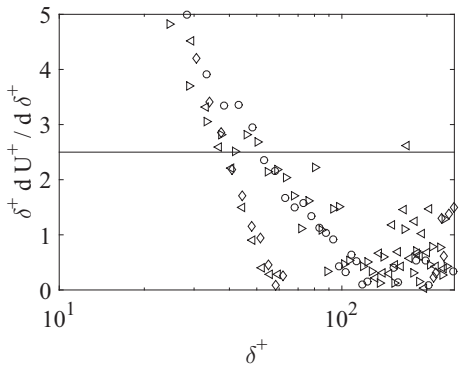

FIG. 4. Logarithmic diagnostic function $\delta^+ \frac{dU^+}{d\delta^+}$ plotted in local wall units against the inner cylinder radial distance δ^+, for different impeller rotational speeds N: ○ 114 rpm, ▷ 90 rpm, ◇ 70 rpm, ◁ 50 rpm; solid line: von Karman κ value.

Taylor (1936), Smith and Townsend (1982). This flat profile of the bulk azimuthal velocity is caused by the advection due to Taylor vortices rather than by turbulent macromixing.

In Fig. 3, the Reynolds averaged azimuthal velocity $\overline{U_\theta}$ is now plotted in semilogarithmic scale and in local wall units U^+ against the radial wall distance δ^+; in classical wall units, the velocity scale U_i^* is the friction velocity induced by the fluid shearing along the inner cylinder and the length scale is ν/U_i^*. In addition, the linear profile of velocity is plotted in the viscous sublayer as well as the classical log law profile. Similar trends have been observed close to the outer cylinder.

In Fig. 3, the Reynolds averaged azimuthal velocity profile does not follow at all the log law. Compared to log law profile, the experimental data present a strong downwards-bending correction, for wall distances ranging between 10 and 100.

Following Grossmann *et al.* [14] and Ostilla *et al.* [24], we plot (Fig. 4) the logarithmic diagnostic function $\delta^+ \frac{dU^+}{d\delta^+}$. A constant value equal to $1/\kappa = 2.5$ should occur for a log law profile. From the figure, it is clear that in our experiment, the logarithmic diagnostic function is not constant at all; it is similar to Ostilla *et al.* [24] (Fig. 6). It is thus appropriate

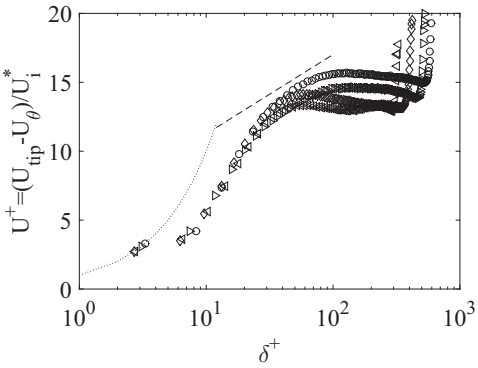

FIG. 3. Reynolds averaged azimuthal velocity U^+ plotted in semilogarithmic scale and in local wall units against the inner cylinder radial distance δ^+ from the inner cylinder, for different impeller rotational speeds N: ○ 114 rpm, ▷ 90 rpm, ◇ 70 rpm, ◁ 50 rpm; dotted line: viscous sublayer; dashed line: logarithmic law.

to look for an explanation, and to revisit the derivation of the velocity profile, which is based on Reynolds averaged Navier-Stokes equations.

In this paper, we shall derive in a first part the profile of turbulent macromixing length from the local momentum balance, injecting the experimental values of Reynolds averaged azimuthal velocity component and then propose an empirical correlation that fits the profile. We shall then inject this analytical expression of the mixing length in the momentum balance in order to derive an analytical expression of the Reynolds averaged azimuthal velocity profile. In a second part, we shall estimate the radial profile of viscous dissipation rate of kinetic energy and compare its spatial averaged value to the global estimation of the power per unit mass needed to rotate the inner cylinder.

III. DISCUSSION

A. Turbulent mixing length

In cylindrical coordinates in such a Taylor-Couette reactor, the RANS equations can be simplified assuming that only the azimuthal velocity component is not null and depends only on the radial position. This momentum equation (4) can be expanded as follows:

$$r^2(\nu + \nu^t) r \frac{\partial \frac{\overline{U_\theta}}{r}}{\partial r} = -r_i^2 U_i^{*2}. \tag{4}$$

Thus, the angular velocity turbulent flux is strictly conserved in a Taylor-Couette flow: $r^2 \tau_{r_\theta}^{\text{tot}} = r_i^2 \tau_{r_{i\theta}}^{\text{tot}}$. Consequently, one should be able to express the mixing length (or the turbulent viscosity, see Appendix) by examining the Reynolds averaged azimuthal velocity profile; in the momentum balance, the gradient of azimuthal velocity can be estimated from PIV data processing. As far as the flow is turbulent, outside the viscous sublayer, one can neglect the molecular viscosity compared to the turbulent one. Different authors investigated the modeling of the turbulent viscosity [8,9,14] in the Taylor-Couette system. The turbulent viscosity can be expressed as

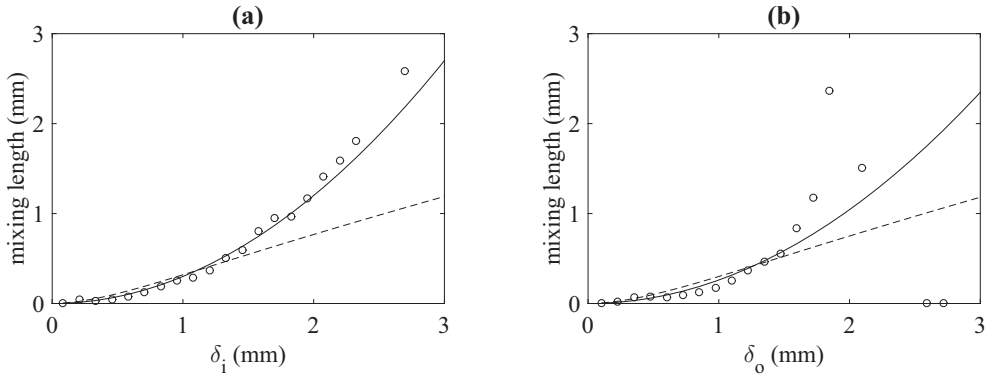

FIG. 5. Turbulent mixing length profile plotted against the wall distance δ from the (a) inner and (b) outer cylinder; ○ numerical data; dashed line: van Driest model; solid line: model corresponding to Eq. (6).

[Eq. (5)] (for further development, see Appendix):

$$\nu^t(r) = l_m^2(r) r \frac{\partial \frac{\overline{U_\theta}}{r}}{\partial r}. \tag{5}$$

In this paper, we propose to focus on the mixing length, introduced by Prandtl. The previous equation can be rewritten and the estimation of the turbulent mixing length profile based on momentum balance as follows [Eq. (6)]:

$$l_m(r) = \frac{r_i}{r^2} \frac{U_i^*}{\frac{\partial \frac{\overline{U_\theta}}{r}}{\partial r}}. \tag{6}$$

The derivation of the turbulent mixing length profile was performed for the different angular velocities. In our case, two turbulent mixing length profiles are plotted close to the inner [Fig. 5(a)] and outer [Fig. 5(b)] walls for the largest angular velocity.

Recall the van Driest expression of the mixing length, where δ is the distance to the wall $l_{mvD}(\delta) = \kappa\delta(1 - e^{-\delta^+/A})$. This relation expresses that far from the wall ($\delta^+ > A$), the mixing length increases linearly with the distance to the wall ($l_{mvD} \approx \kappa\delta$) whereas closer to the wall, there is a correcting factor. Far from the wall, the profile of velocity is logarithmic, as confirmed by experiments performed for highly turbulent flow [13]. Recall that in the analysis of the azimuthal velocity in terms of classical logarithmic law, it was pointed out that von Karman constant κ should take values slightly modified compared to the channel flow. At medium Reynolds numbers, the logarithmic profile is not observed (Fig. 3). As far as $\delta^+ < A$, the van Driest mixing length expression can be approximated by $l_{mvD}(r) = (\kappa)/A(\delta^2 U^*)/\nu$. In our case, the turbulent mixing length profiles plotted close to the inner and outer walls are plotted on Fig. 5. Considering the mixing length profiles close to the inner and outer walls for the four angular velocities, processed data exhibit a similar trend that can be modeled as a function of the wall distances ($\delta_i = r - r_i; \delta_o = r - r_o$).

$$l_{mi}(r) = C_l \frac{\delta_i^2 U_i^*}{\nu}, \tag{7}$$

$$l_{me}(r) = C_l \frac{\delta_o^2 U_o^*}{\nu}. \tag{8}$$

The same value of the constant $C_l = 0.0075$ fits the profiles of mixing length close to the inner and outer walls. It is interesting to point out that the trend of our model is similar to van Driest one, but the value of our constant C_l is half the ratio κ/A, considering classical values of von Karman constant κ and A in channel flow. This confirms that the mixing length profile is nonlinear (quadratic) with respect to the radial distance to the inner and outer walls.

B. Mean velocity profile close to the walls

It is now possible to derive an analytical expression of the Reynolds averaged azimuthal velocity profile. Recall the RANS equation:

$$r^3 \frac{\partial \frac{\overline{U_\theta}}{r}}{\partial r} l_m(r) = -r_i U_i^*. \tag{9}$$

After injecting the mixing length $l_{mi}(r) = C_l \frac{\delta_i^2 U_i^*}{\nu}$, one obtains:

$$\frac{\partial}{\partial r}\left(\frac{\overline{U_\theta}}{r}\right) = \frac{-r_i \nu}{C_l r^2 (r - r_i)^2}. \tag{10}$$

This can be easily integrated; after derivation, one obtains:

$$\frac{U_{\text{tip}} - \overline{U_\theta}(r)}{U_i^*} = -\frac{1}{C_l r_i^+} \frac{r_i - 2r}{\delta_i} + \frac{2}{C_l r_i^+} \frac{r_i + \delta_i}{r_i} \log\left(\frac{\delta_i}{r_i + \delta_i}\right) + \frac{C_U(r_i + \delta_i)}{U_i^*}. \tag{11}$$

where U_{tip} is the velocity of the internal cylinder ($U_{\text{tip}} = r_i\omega$). The mean velocity profiles are plotted in Fig. 6, for the two rotational velocity of the impeller. The value of the constant C_U is close to $U_{\text{tip}}/2$. In addition, the ratio of the first term of the right-hand side ($\mathcal{R}1$) of the velocity expression over the second one ($\mathcal{R}2$) can be expressed as:

$$\frac{\mathcal{R}1}{\mathcal{R}2} = \frac{1}{2}\frac{r_i}{r}\frac{1 - \frac{\delta_i}{r}}{\frac{\delta_i}{r}} \frac{1}{\log\left(1 + \frac{r_i}{\delta_i}\right)} \tag{12}$$

In our experiment, the ratio δ_i/r is less than $d/r_i = 0.15$. Thus, the ratio $\mathcal{R}1/\mathcal{R}2$ is large and it is not surprising that the Reynolds averaged azimuthal velocity profile significantly

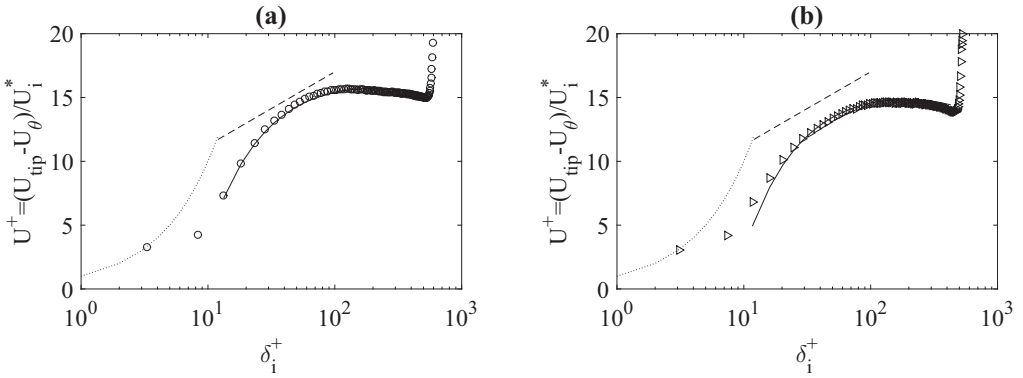

FIG. 6. Reynolds averaged azimuthal velocity U^+ plotted in semilogarithmic scale and in local wall units against the inner cylinder radial distance δ^+ from the inner cylinder (a) = ($\circ$ $N = 114$ rpm, Re $\cong$ 18000, $C_U = 5.1$) and (b) = ($\triangleright$ $N = 90$ rpm, Re $\cong$ 14000, $C_U = 3.9$); dotted line: viscous sublayer; dashed line: logarithmic law.

departs from a log law profile. Indeed, in our experiment, the velocity profile evolves as the inverse of the distance to the cylinder. In a different geometry, such as Huisman *et al.* [13], the geometrical ratio d/r_i is up to 0.4 and thus the logarithmic term ($\mathcal{R}2$) may have the same order of magnitude as the first term ($\mathcal{R}1$). In addition, in the case of high Reynolds number investigated by these authors, the expression of the mixing length should be modified: the van Driest type expression should be substituted to the simplified quadratic expression [Eq. (6)], that we have proposed at medium Reynolds number.

In order to validate our model, a similar data processing was applied to Huisman *et al.* [13] data from Twente turbulent Taylor-Couette (T3C). Their inner cylinder radius is 0.2 m, the outer one is 0.279, leading to a radius radio equal to 0.716. Three profiles of azimuthal velocity have been selected to illustrate the efficiency of our model ($N = 120$, 60, and 30 rpm). The turbulent mixing length has been deduced from the experiments. It is plotted on Fig. 7. Clearly, in the region close to the wall ($\delta_i^+ < 50$), the mixing length is quadratic, similarly to our experiments; however, further away ($\delta_i^+ > 50$), the mixing length becomes linear ($\kappa = 0.6$). Such behaviors are similar to van Driest one, but the constants fitting the experimental data are different from classical ones.

Given this mixing length, one can calculate the azimuthal velocity profile, following our approach. The velocity profiles

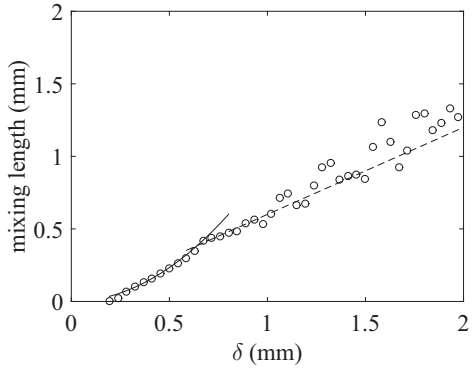

FIG. 7. Turbulent mixing length profile plotted against the wall distance δ from the inner cylinder, $\circ$ Twente turbulent Taylor-Couette (T3C) data (Re $= 2 \times 10^5$), dashed line: linear expression based on $\kappa = 0.6$ and solid line: quadratic model based on $C_l = 0.0125$.

are plotted in Fig. 8. Clearly again, in the region close to the wall ($\delta_i^+ < 50$), the Reynolds averaged azimuthal velocity profile is not logarithmic for each of the inner cylinder velocity ($N = 120$, 60, and 30 rpm) but is well predicted by our model ($C_U = 6.75$, 3.2, and 1.55); however, further away ($\delta_i^+ > 50$), the Reynolds averaged azimuthal velocity profile becomes logarithmic but the constants can be estimated and they are not the classical ones ($B = 7.45$, 7.1,6.2; $\kappa = 0.6$). It appears from the different plots that the constant C_U varies with both the geometry and the rotational speed. Clearly, the value of the constant C_U is proportional to the rotational speed. Additional work is needed to generalize the present approach.

C. Global characteristics

Our purpose is now to estimate local and global values of the viscous dissipation rate of total kinetic energy. It is composed of two terms, the viscous dissipation rate of mean flow kinetic energy and viscous dissipation rate of turbulent kinetic energy. In the viscous sublayer, the viscous dissipation rate of kinetic energy is reduced to the mean flow and it can be derived analytically; it is roughly constant:

$$\epsilon_{iVSL}(r) = \frac{U_i^{*4}}{\nu}\left(\frac{r_i}{r}\right)^2 \approx \frac{U_i^{*4}}{\nu}, \tag{13}$$

$$\epsilon_{oVSL}(r) = \frac{U_o^{*4}}{\nu}\left(\frac{r_o}{r}\right)^2 \approx \frac{U_o^{*4}}{\nu}. \tag{14}$$

Outside the viscous sublayer, the radial profile of viscous dissipation rate of mean flow kinetic energy can be estimated from the measurement of the Reynolds averaged azimuthal velocity:

$$\epsilon_{MF}(r) = \nu\left[r\frac{\partial\left(\frac{\overline{U_\theta}}{r}\right)}{\partial r}\right]^2. \tag{15}$$

Following our approach based on turbulent viscosity, one can estimate the production of turbulent kinetic energy:

$$\mathcal{P}_{\mathrm{TKE}}(r) = \nu^t(r)\left[r\frac{\partial\left(\frac{\overline{U_\theta}}{r}\right)}{\partial r}\right]^2 = \frac{r_i^2}{r^2}U_i^{*2}\left[r\frac{\partial\left(\frac{\overline{U_\theta}}{r}\right)}{\partial r}\right] - \epsilon_{MF}(r). \tag{16}$$

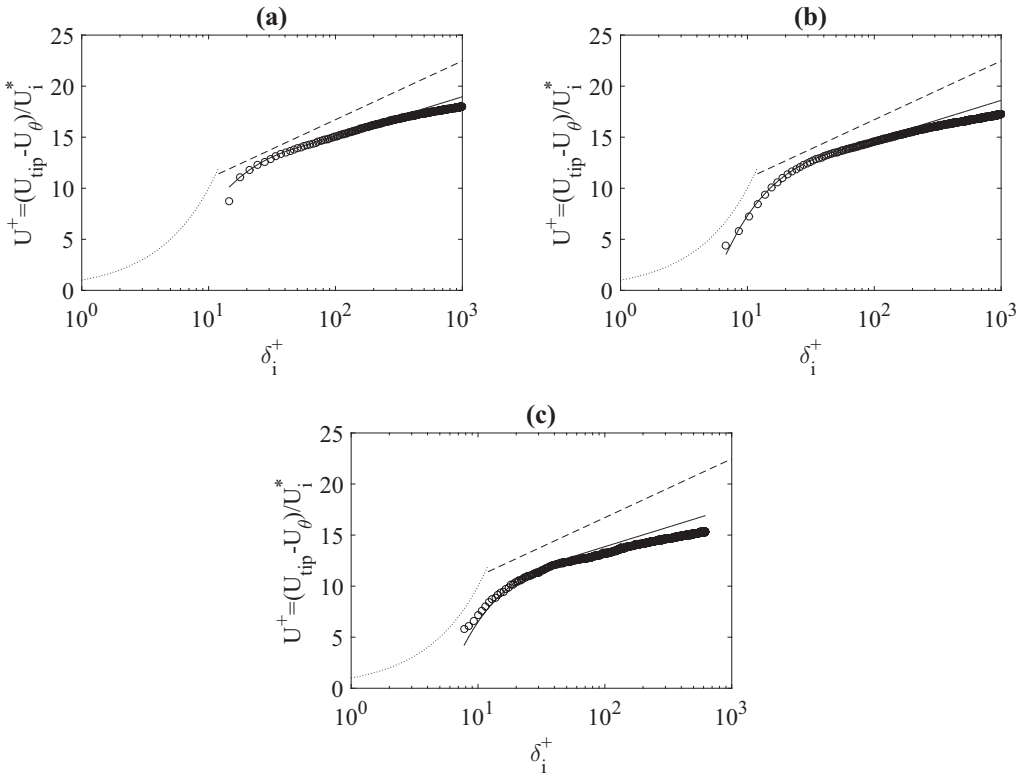

FIG. 8. Reynolds averaged azimuthal velocity U^+ plotted in semilogarithmic scale and in local wall units against the inner cylinder radial distance δ^+ from the inner cylinder, ○ Twente turbulent Taylor-Couette (T3C) data (a) ($N = 120$ rpm, Re $\cong$ 200 000, and $C_U = 6.75$, (b) ($N = 60$ rpm, Re $\cong$ 100 000, and $C_U = 3.2$) and (c) ($N = 30$ rpm, Re $\cong$ 50000, and $C_U = 1.55$); dotted line: viscous sublayer; dashed line: logarithmic law.

The resolution of our PIV systems being limited to estimate directly the viscous dissipation rate of turbulent kinetic energy, we will consider, in this paper, an equilibrium between production and dissipation of turbulent kinetic energy, and thus deduce the viscous dissipation of TKE from the production term. These three terms are nondimensionalized by the viscous dissipation rate of kinetic energy at the inner cylinder (U_i^4/ν). Such terms are plotted on Fig. 9 against the wall distance δ expressed in local wall units. The total viscous dissipation of kinetic energy (VDKE) results from the sum of the mean flow VDKE and the turbulent VDKE.

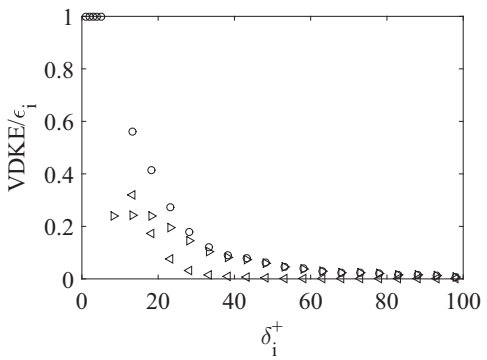

FIG. 9. Viscous dissipation of kinetic energy profile divided by its inner wall value ϵ_i against the inner cylinder radial distance δ^+ from the inner cylinder ($N = 114$ rpm): ▷ TKE production; ◁ mean KE dissipation; ○ total KE dissipation.

At radial position δ_i^+ larger than 15, the turbulent part of viscous dissipation rate of kinetic energy dominates whereas close to the wall, $\delta_i^+ < 15$, the viscous dissipation rate of mean flow kinetic energy dominates. In the viscous sublayer, the local value of viscous dissipation rate of mean flow kinetic energy is roughly constant $\epsilon_i = U_i^{*4}/\nu$ and five times larger than the viscous dissipation rate of turbulent kinetic energy at $\delta_i^+ = 20$. Based on these profiles, one can estimate the mean value the total viscous dissipation rate of total kinetic energy (mean flow plus turbulent flow) and one obtains 0.137 W/kg. This value is very close to the average value estimated in Table I. Similar result can be obtained with at other rotational speeds.

IV. CONCLUSIONS

In this paper, we confirm that the azimuthal velocity profiles do not follow a log law at medium Reynolds numbers; we deduce from the PIV measurements and momentum balance an estimation of the mixing length profile. We confirm nonlinear dependence of the turbulent mixing length with respect to the distance to the wall and we propose a law of the azimuthal velocity close to the cylinders. Indeed, in our experiment, the velocity profile evolves as the inverse of the distance to the cylinder. This model is validated by comparison to Huisman data. In the second part, we derived the viscous dissipation rate

profile of the mean flow kinetic energy and we estimated the viscous dissipation rate profile of the turbulent kinetic energy, assuming equilibrium between production and dissipation of turbulent kinetic energy. Finally, the average value of radial profile of viscous dissipation rate of total kinetic energy is estimated and shown to be close to the estimation $\langle\epsilon\rangle$ based on Wendt correlation of the torque.

ACKNOWLEDGMENTS

H.S. would like to acknowledge the importance of the Conselho Nacional de Desenvolvimento Cientifico e Tecnologico (CNPq), Brasil, for support through the postgraduate (Process No. 140756/2012-4) and "Doutorado Sanduíche" (Process No. 241739/2012-8) Scholarship programs. We would also like to thank Sanders Huisman for providing his PIV data of his article [13], thus reducing significant amount of error, which would have occurred due to the manual extraction from the figures.

APPENDIX

The estimation of the turbulent viscosity profile based on momentum balance was performed for the different angular velocities. Considering the turbulent viscosity profiles close to the inner and outer walls for the four angular velocities, processed data exhibit a similar trend that can be modeled as $1 + \nu^t/\nu = \delta_i^{+2}/C_\nu$. Between wall scale distances from 1–50, the empirical quadratic expression for the turbulent viscosity is similar to the classical expression proposed by van Driest, with different constant value. Our simplified expression enables us to give an analytical solution for the turbulent viscosity $\nu^t(r) = (r - r_i)U_i^*(\delta_i^+)/C_\nu \approx \kappa(r - r_i)U_i^*[1 - e^{(-\delta_i^+/A)}]^2$. This expression was found to fit correctly the turbulent viscosity profile issued from experimental data, given adapted C_ν values.

[1] C. Coufort, D. Bouyer, and A. Line, Chem. Eng. Sci. **60**, 2179 (2005).
[2] M. Vlieghe, C. Coufort-Saudejaud, C. Frances, and A. Liné, Am. Inst. Chem. Eng. J. **60**, 2389 (2014).
[3] E. Imomoh, J. Dusting, and S. Balabani, Phys. Fluids **22**, 044103 (2010).
[4] A. Chouippe, E. Climent, D. Legendre, and C. Gaillet, Phys. Fluids **26**, 043304 (2014).
[5] D. R. Gabe, G. D. Wilcon, J. Gonzalez-Garcia, and F. C. Walsh, J. Appl. Electrochem. **4**, 91 (1998).
[6] B. Haut, H. Ben Amor, L. Coulon, A. Jacquet, and V. Halloin, Chem. Eng. Sci. **58**, 777 (2003).
[7] M. Douaire, M. Mercade, J. Morchain, and P. Loubiére, Biotechnol. Bioeng. **108**, 559 (2010).
[8] D. Richard and J. P. Zahn, Astron. Astrophys. **347**, 734 (1999).
[9] S. Mathis, A. Palacios, and J. P. Zahn, Astron. Astrophys. **425**, 243 (2004).
[10] H. Ji, M. Burin, E. Schartman, and J. Goodman, Nature (London) **444**, 343 (2006).
[11] M. A. Fardin, C. Perge, and N. Taberlet, Soft Matter **10**, 3523 (2014).
[12] S. Grossmann, D. Lohse, and C. Sun, Annu. Rev. Fluid Mech. **48**, 53 (2016).
[13] S. G. Huisman, S. Scharnowski, C. Cierpka, C. J. Kähler, D. Lohse, and C. Sun, Phys. Rev. Lett. **110**, 264501 (2013).
[14] S. Grossmann, D. Lohse, and C. Sun, Phys. Fluids **26**, 025114 (2014).
[15] M. Kobayashi, H. Maekawa, T. Takano, and Y. Yamada, JSME Int. J. II **33**, 436 (1990).
[16] S. T. Wereley and R. M. Lueptow, Exp. Fluids **18**, 1 (1994).
[17] J. Parker and P. Merati, J. Fluids Eng. **118**, 810 (1996).
[18] F. Wendt, Ing. Arch. **4**, 577 (1933).
[19] B. Dubrulle and F. Hersant, Eur. Phys. J. B **26**, 379 (2002).
[20] M. S. Paoletti, D. P. M. van Gils, B. Dubrulle, C. Sun, D. Lohse, and D. P. Lathrop, Astron. Astrophys. **547**, A64 (2012).
[21] G. S. Lewis and H. L. Swinney, Phys. Rev. E **59**, 5457 (1999).
[22] G. P. Smith and A. A. Townsend, J. Fluid Mech. **123**, 187 (1982).
[23] R. Ostilla Mónico, R. J. A. M. Stevens, S. Grossmann, R. Verzicco, and D. Lohse, J. Fluid Mech. **747**, 1 (2014).
[24] R. Ostilla Mónico, R. Verzicco, S. Grossmann, and D. Lohse, J. Fluid Mech. **788**, 95 (2016).
[25] D. Pirro and M. Quadrio, Eur. J. Mech. B Fluid. **27**, 552 (2008).
[26] D. P. Lathrop, J. Fineberg, and H. L. Swinney, Phys. Rev. A **46**, 6390 (1992).